Apparent Attenuation Beneath the United States and its Correlation with Lithospheric Provinces

A THESIS
SUBMITTED TO THE FACULTY OF
UNIVERSITY OF MINNESOTA
BY

Sara Kowalke

IN PARTIAL FULFILLMENT OF THE REQUIREMENTS
FOR THE DEGREE OF
MASTER OF SCIENCE

Maximiliano Bezada

September, 2016

Acknowledgements

Seismic data used in this study are available through IRIS-DMC (http://ds.iris.edu/ds/nodes/dmc/). I appreciate the work of those who installed and maintained the USArray Transportable Array for their role providing unprecedented seismic data of the United States.

Additionally, I would like to express my sincere gratitude to my advisor, Dr. Max Bezada, for the support, guidance, and knowledge he provided me throughout my thesis. I would like to thank the rest of my thesis committee, Dr. Justin Revenaugh and Dr. Peter Hudleston, for their critical review of my thesis.

Last, but not least, I thank my family for their unrelenting encouragement and support not only during this thesis, but in all aspects of my life.

Abstract

We map apparent attenuation beneath the continental United States through time-domain waveform analysis of 19 deep-focus teleseismic events recorded by the USArray Transportable Array. Results show good correlation with lithospheric boundaries. Low t* is common across the cratonic continent and high t* regions dominate in the western U.S. and east of the Appalachian front. Some geographic variations are not consistent with expectations, such as relatively low t* in the North Basin and Range. Comparisons with additional techniques, including heat flow, tomography, and seismicity, indicate regional influence of non-thermal attenuation factors. Different lithospheric provinces have distinct attenuation signatures that assist in understanding the behavior of the lithospheric continent.

Table of Contents

List of Figures

1 Introduction

Most modern geologic patterns are a direct consequence of lithospheric plate interactions. The Wilson Cycle illustrates processes, such as extensional rifting, collisional thrusting, and subduction, which are responsible for the evolution of continents on a global scale. Interpreting the nature and rates of tectonic processes responsible for lithospheric construction and destruction are vital to develop a well-rounded understanding of continental structures. Plate tectonic theories demonstrate great success in predicting oceanic phenomena, however, their continental expressions are more complex (Atwater, 1970). In order to grasp the intricacies of their interactions, we focus on North America since all of these processes combined to give rise to its modern configuration and a great deal is known about its features.

The architecture of the North American continent has exhibited several phases of growth and destruction, making it an ideal subject of study. Understanding the assemblage of North America provides constraints on continental structure that can be used to draw conclusions about continental lithospheric behavior. Numerous papers offer a comprehensive overview of the tectonic evolution of North America (e.g., Hoffman, 1988; Corrigan et al., 2005; Whitmeyer and Karlstrom, 2007). The continental core of North America is the craton, assembled during the Archean and Paleoproterozoic eras (4.0-1.8 Ga) by continent plate collisions. Archean provinces, such as the Superior province and Wyoming province, among others, were amalgamated to the cratonic core during the Trans-Hudson orogeny (1.9-1.8 Ga)(Hoffman, 1988). Much of the present-day U.S. was then constructed by a series of orogenic events, giving rise to major northeast-

trending provinces (Karlstrom and Bowring, 1988). The Yavapai orogeny was the earliest (1.80-1.70 Ga) and created the Yavapai province. Next, the Mazatzal orogeny (1.65-1.60 Ga) formed the Mazatzal province. The Granite-Rhyolite event (1.50-1.30 Ga) followed and formed from intracratonic magmatism. The Grenville orogeny (1.30-0.95 Ga) developed the Grenville and Llano provinces and concluded the history of accretionary orogenesis for Laurentia (Moores, 1991).

All of these accretionary provinces consist of sub terranes separated by shear zones. Following the accretionary period, intracratonic extension and magmatism associated with slab roll-back activated breakup within Laurentia (Whitmeyer and Karlstrom, 2007). One such stage of this breakup is marked by the Argentina Precordillera terrane rifting from the Ouachita embayment region of southeastern Laurentia, creating a destructive boundary in what is presently the central-southern U.S. The combination of these processes to construct North America provokes consideration about the effects the assembly has on lithospheric parameters.

The accretionary provinces created during the Archean and Proterozoic influenced subsequent magmatism and tectonics that reworked the lithospheric structure, primarily in the western U.S. Mafic magmatism and rifting occurring ~1.1 Ga developed along new north-south fracture zones, such as the Rocky Mountain front, and reflects deformation of Laurentian lithosphere at a high angle to the Grenville orogeny (Karlstrom and Humphreys, 1998). These rifting processes thinned the crust and mantle in the western U.S., creating weaker lithosphere. Mantle reorganization persists in the Rocky Mountain region, creating zones of partially molten mantle underlying western

provinces, such as the Snake River Plain and Rio Grande Rift (Karlstrom and Humphreys, 1998).

The western U.S. experienced further deformation during the Laramide tectonism (75-45 Ma) and subsequent Tertiary modification due to the shallow-dipping subduction of the Farallon plate (Karlstrom and Humphreys, 1998). Regional crustal and lithospheric properties determine the deformation style experienced by the area. Post-Laramide tectonics resulted in Tertiary modification. Consequent magmatism from the Farallon slab detachment increased mantle buoyancy and resulted in regional uplift, namely in the Rocky Mountain-Colorado Plateau region. Conversely, the Basin and Range province and Rio Grande Rift experienced intense extension due to previous episodes of mantle deformation (Humphreys and Dueker, 1994). Compositional and mechanical heterogeneities influence the regional response to tectonic stresses and are likely inherited, to some extent, from the lithospheric "grain" generated by northeast-trending Proterozoic provinces (Karlstrom and Humphreys, 1998).

Surface geology and geochemistry reveal many valuable insights about continents, but we rely on indirect geophysical observations for the present-day structure of the subsurface. The U.S. has been explored using various techniques for decades but recently the availability of massive amounts of data collected by Earthscope has allowed for higher resolution than ever before. U.S. heat flow studies (e.g., Blackwell, 1971, 1991; Roy et al., 1972; Sass et al., 1971; Morgan and Gosnold, 1989) characterize geothermal features across the continent and associate them to lithospheric thermal regimes. Body wave tomography studies in the U.S. afford new constraints on lateral

heterogeneities, specifically highlighting residual structures from passive margin volcanism and slab remnants (Goes and van der Lee, 2002; Schmandt and Lin, 2014). Some lithospheric provinces are evident in velocity images, such as the Rocky Mountain front, and Precambrian rift margins. Attenuation offers sensitivity to parameters beyond velocity and heat flow, and therefore, can reveal additional information about the structure of the continent.

Attenuation quantifies the effects of fractional energy loss per cycle based on seismic wave amplitude. There are several factors that may contribute to attenuation, including temperature, hydration, grain size, and partial melt (Jackson et al., 1992, 2002; Hammond and Humphreys, 2000; Karato, 2003; Faul and Jackson, 2005). There is ongoing debate as to the degree of influence each of these factors has on attenuation, but it has long been noted there is often a strong relationship between temperature and attenuation (e.g., Jackson et al., 1992, 2002; Karato, 2003). In the U.S., therefore, the cold cratonic crust can be expected to be high Q, whereas hotter regions in the eastern and western parts of the continent generally exhibit lower Q.

Discerning elastic attenuation from anelastic attenuation contributions can be a major challenge in attenuation studies. Elastic attenuation refers to geometric spreading and scattering of energy; whereas anelastic attenuation, commonly referred to as intrinsic attenuation, is the dispersion of energy in the form of heat (Cafferky and Schmandt, 2015). It is difficult to distinguish sources of attenuation from general regional heterogeneities due to the complex nature of attenuating factors.

Placing robust constraints on Q can be difficult. Most available models are global scale and lack resolution in the continents (e.g., Selby and Woodhouse, 2002; Warren and Shearer, 2002; Gung and Romanowicz, 2004; Dalton et al., 2008). Global Q models using surface wave attenuation can be regionally inconsistent, due to results being averaged over fairly large areas (Mitchell, 1995). Subduction zone studies utilize body wave data and typically have better resolution because of higher frequency of earthquakes (e.g., Roth et al., 1999; Wiens et al., 2008), but available continental models are not as regionally consistent as other techniques, such as tomography. Short-period body waves allow more localized measurements than surface wave studies and are often used to resolve regional heterogeneities in Q measurements (Mitchell, 1995). In a recent study, Cafferky and Schmandt (2015) use frequency-domain P-wave amplitude spectra to generate a map of Δt^* in the U.S. that largely follows anticipated trends with lowest Δt^* in the Midwest and higher Δt^* values in the east and west. However, there are regions, such as the Superior Craton, that are inconsistent with expectations and these inconsistencies are attributed to scattering. Scattering effects interfere with attenuation signals and develop regional variations that are not well explained by thermal effects. We sidestep these scattering challenges using a new technique set in the time-domain. Time-domain waveform modeling results in fewer effects from scattering because traces exhibiting strong scattering are inherently excluded from the study due to poor fit with event source estimates.

The availability of new data resulting from the deployment of the dense USArray Transportable Array (US-TA) is a valuable resource for seismic studies in the U.S. US-

TA data enabled us to conduct a regional attenuation study in the contiguous U.S. We generated a map of apparent attenuation beneath the U.S. using a time-domain technique for 19 deep-focus teleseismic events. The resulting map largely follows anticipated trends; however, there are some intriguing regional attenuation patterns that do not match expectations. We aim to attribute the observed attenuation signatures to the tectonic processes that dictate the construction and destruction of the continent.

2 Methods

2.1 Data

We utilize a time-domain waveform modeling approach to estimate t*. We extract the regional attenuation pattern through an analysis of deep-focus teleseismic events recorded by the dense US-TA. Figure 1A shows the distribution of stations from US-TA used for this study. We employ a magnitude range of Mw5.5-7.0 where waveforms are impulsive, simple, have sufficiently large signal-to-noise ratios, and can be modeled. Deep-focus events are especially useful because they experience attenuation mostly on the receiver side, therefore, we restricted estimated focal depth to 400-650 km for candidate events. We also applied further restriction by requiring azimuthal distances of 30-90° to avoid P-wave triplication complexity. US-TA provides dense coverage over the entire study area. Broadband seismograms for the events meeting these criteria during USArray deployment (2005-2014) were obtained from IRIS-DMC. Of the 39 events that met the criteria, 19 events were hand-picked for the study because they displayed the highest signal to noise ratio and simplicity of the source (Figure 1B).

2.2 Estimating t*

Once the 19 events were chosen for the study, the source was estimated from a stack of recordings displaying the sharpest P-waves since these are the least attenuated traces (Figure 2). Because we are matching the shape of the primary pulse, the estimate is not sensitive to the shape of the coda, which may help reduce its sensitivity to scattering or the effects of elastic attenuation. An attenuation operator was applied to the source estimates using a range of t* values to fit the recordings at each station. We use the attenuation operator with an exponential decay in amplitude and the dispersion relation proposed by Azimi et al. (1968). The full operator *O* is defined as follows:

$$O = \exp\left\{-\omega t^{*} \cdot \left[\frac{1}{2} + \frac{i}{\pi}\ln\left(\frac{\omega}{\omega_0}\right)\right]\right\}$$

Where ω is the angular frequency and ω_0 is the reference (unrelaxed) frequency. We note that the attenuation operator is applied in the frequency domain but the misfit with respect to the observed waveform is determined in time domain by comparing the observed and attenuated source estimate. The records at each station were reviewed and any traces demonstrating a poor fit were not included in the study (Figure 3**)**.

2.3 Inversion scheme

An inversion scheme was applied for t* at nodes evenly spaced 50km apart. Observations at each node are the weighted average of the values of the surrounding nodes within a 100km radius, plus the station term (Figure 4A) and event term for each event-station pair. Each weight is the inverse of the corresponding node-to-observation distance. The inversion is regularized by imposing smoothness and smallness constraints

on the model. Choosing the regularization constraints was based on visual inspection of the results to smooth the model without sacrificing resolution of the results. Figure 4B shows the smoothed t* inversion map of all 19 events.

2.4 Jackknife test

After the t* map was generated, a jackknife test was performed to confirm the robustness of the regional attenuation patterns (Figure 5A). Due to the relatively small number of events, we use this test to understand the effect of event selection on the resulting attenuation map. We stacked and took the mean of 100 random combinations of 10 of the 19 events and we see the predominant pattern does not display much variation from the smoothed map showing all of the events. The standard deviation map (Figure 5B) shows low variation, especially in the cratonic core. Low standard deviation corresponds to consistent geographic variations regardless of event selection. We also performed the same jackknife test using combinations of 14 of the 19 events (Figure 6A&B) and observe essentially the same result, further indicating that event selection does not have a strong impact on the resulting geographic variations.

3 Results

The major geographic variations in apparent attenuation are generally consistent, with some noteworthy exceptions. The lowest apparent attenuation occurs in the upper Midwest, whereas high apparent attenuation dominates outside the cratonic continent, namely to the west. East of the Appalachian front also shows relatively high apparent attenuation, except for a block occupying North Carolina and South Carolina. Although

the general pattern matches expectations, there are several regions that display intriguing patterns inconsistent with anticipated results.

The region of low t* in the central U.S. appears well defined by prominent lithospheric boundaries (Figure 7). It is bounded by the Trans-Hudson on the west and the Appalachian Front to the east. To the south, there appears to be more of a gradual transition to higher t*, but the boundary is still oriented parallel to the rifting section of the Appalachian Front that defines the Ouachita embayment. The low t* region crosscuts the NE/SW-trending Precambrian accretionary boundaries, but does not cut across the destructive rifting boundary in the south central part of the continent.

While the western U.S. is generally high t*, it is not uniformly so. The Rocky Mountain Front defines the eastern extent of high t* regions in the western U.S. There are three main regions displaying the highest t* values that form a "C" pattern on the attenuation map. The Rio Grande Rift, north-western corner of the U.S., and southern California exhibit high t* measurements. All three of these regions are currently experiencing tectonic activity associated with high heat flow and low upper mantle velocities.

The North Basin and Range stands out as an exception to the western patterns as it displays relatively low t* values. Since many authors identify temperature as the main control on attenuation, one would anticipate high t* in this region; however, our results suggest relatively low attenuation.

Another area of particular interest is the Ouachita embayment. This area experienced rifting of the Argentina Precordillera province and left behind long arms of

failed rifts that expanse much of the south central U.S. (Whitmeyer and Karlstrom, 2007). This region of relatively high t* is consistent with areas of low upper mantle velocity and high heat flow (e.g., Blackwell et al., 1991; Schmandt and Lin, 2014). The transition from low t* in the craton to higher t* south of the failed rifts indicates possible links between attenuation and lithospheric strength.

Wyoming's attenuation patterns illuminate the complicated tectonic history of the region. The Rocky Mountain front runs through Wyoming, and as such, one would anticipate the section west of the front to display high attenuation. However, we see a NE/SW-trending gap in high attenuation west of the front. Similar gaps have been observed in heat flow and tomography studies (e.g., Blackwell et al., 1991; Schmandt and Lin, 2014).

4 Comparisons with other observations

In this section we compare and contrast our results with different observations pertaining to specific areas of interest. Relating our results to observations regarding heat flow, volcanism, and seismicity provides insight into the processes that control attenuation and explain regional variations of t* across the U.S.

4.1 Heat flow

Upper mantle thermal structure is relatively well constrained across the U.S. due to wave speed tomography and heat flow measurements. The SMU Geothermal Laboratory generated an updated heat flow map of the continental U.S. in 2011 using data from National Geothermal Data Systems (NGDS) (Blackwell et al., 2011). Figure 8 depicts the same heat flow measurements from NGDS reprocessed in order to be

consistent with our grid, and with a low-pass smoothing filter applied to visually match the SMU heat flow map.

The heat flow map displays a similar overall pattern to the apparent attenuation map, with some key exceptions. Temperature is known to affect Q and thus, we would expect the two to be highly correlated. This is particularly apparent in several locations where attenuation patterns show high agreement with the heat flow map, such as Wyoming, the Ouachita embayment, and the Rio Grande Rift. However, there is only partial correlation ($r = 0.502$) between apparent attenuation and heat flow measurements, indicating thermal control does not dominate everywhere. For instance, in the western U.S. the North Basin and Range region, previously mentioned to demonstrate relatively low t*, shows consistently high heat flow due to the active tectonics in the area. There are many regional heterogeneities that cannot be attributed solely to the influence of heat flow, implying attenuation can be regionally controlled by other parameters.

4.2 Volcanism

Western North America has a complex history of volcanism due to past and present tectonic processes. The evolution of the Pacific-North American-Farallon plate boundary certainly influences the patterns of magmatism and extension (McQuarrie and Oskin, 2010). We utilize data from the North American Volcanic Database (NAVDat, navdat.geongrid.org) to relate space-time distribution of Cenozoic volcanism (42-0 Ma) to patterns of apparent attenuation (Figure 9)(Walker et al., 2004). The data are split into two time frames, the older being 45-21 Ma, and the more recent volcanism is 20-0 Ma. The older volcanism period is largely attributed to a rapidly migrating arc/backarc system

(Dickinson, 2002). The more recent period of volcanism is a result of the early Cascade arc system or the slab window resulting as the triple junction moved to the north (McQuarrie and Oskin, 2010).

Volcanism appears to occur around the areas of highest attenuation, but not directly in them. The Rio Grande Rift, Southern California, Snake River Plain, and North Basin and Range regions show especially interesting patterns.

The Rio Grande Rift demonstrates a unique pattern of past and present magmatism (Figure 10). The area displays volcanism north and south of the high attenuation region in New Mexico until very recently. Two clusters from the earlier magmatic episode (45-21 Ma) bound the region displaying highest t*. This pattern is made particularly clear in Figure 10C, where the igneous sample ages are plotted with the t* estimates along the A-A' transect. The gap in early magmatism is generally consistent with the location of high t*. More recent magmatism fills the gap and falls within the high t* area.

Similarly, Southern California lacks evidence of early magmatism in the high t* area. There is limited magmatism from the early episode to the northwest and southeast of the most attenuating region. Magmatic events from the more recent episode occur throughout eastern California with no bias toward the high t* area.

Another area demonstrating noteworthy magmatism patterns is north of the Snake River Plain region. Analogous to Rio Grande and Southern California, there is little to no magmatism from the early magmatic episode in the region of highest t* north of Snake River Plain. Unlike southern California and Rio Grande Rift, there is very limited

magmatism from the more recent episode inside the attenuating region, as well. However, there is dense magmatism along the Snake River Plain lining the southern boundary of the highly attenuating area.

The North Basin and Range exhibits a different pattern. There is ample magmatism originating from the early magmatism episode. However, there is no recent magmatism where t* is relatively low compared to its surroundings. Recent magmatism is concentrated around the North Basin and Range, especially in the Snake River Plain area and eastern California.

4.3 Seismicity

The distribution of earthquakes throughout the U.S. creates some striking patterns when overlain on our attenuation map. Using data from USGS catalogs, we plotted epicentral locations for 10,000 earthquakes spanning from 1996-2016 (Figure 11). Overall, seismicity tends to concentrate at the edges of the t* provinces. Seismicity clearly dominates in the western U.S. due to its continued tectonic activity, however, there appears to be a correlation between the patterns of attenuation and earthquake locations. The bulk of the seismicity occurs outside the low attenuation region in the central U.S. In the northwest U.S., earthquakes are concentrated on the outside of the high t* region north of Snake River Plain. With the exception of Southern California, there is limited seismicity within the peak attenuation areas in the northwestern corner of the U.S. and the Rio Grande Rift. There is a ring of seismic activity circling the North Basin and Range. In the eastern U.S., much of the seismicity falls along or near the

Appalachian front. There is also seismicity concentrated on the southern edge of the low t* block in North and South Carolina.

5 Discussion

When interpreting these results, it is important to note the t* estimates are an aggregate of attenuation anomalies beneath each station and may represent separate anomalies at different depths in the upper mantle. Nevertheless, our results reveal some intriguing points regarding lateral t* variations across the U.S.

5.1 Magnitude of t* variations

The magnitudes of our t* variations are larger than some models suggest, but are generally on track with current studies. Global surface wave Q models (e.g., Selby and Woodhouse, 2000; Romanowicz, 1995) resolve lower variation magnitudes consistent with expected upper mantle Q structure of PREM (Dziewonski and Anderson, 1981). Body wave studies (e.g., Warren and Shearer, 2002; Hwang et al., 2011; Cafferky and Schmandt, 2015) obtain larger lateral variations. Our inverted t* magnitudes are slightly smaller than those found in Warren and Shearer (2002) and Cafferky and Schmandt (2015), but are still larger than those found in surface wave models. The trend of higher t* magnitudes in recent studies could arise from the availability of data from the more dense US-TA. Furthermore, variations in t* magnitudes could indicate the possibility of non-thermal intrinsic attenuation contributions that have an amplifying effect, such as partial melt and hydration.

In order to check the plausibility of our t* estimates, we used the Q_p and V_{pv} structure from PREM (Dziewonski and Anderson, 1981) to determine the approximate

lithosphere-asthenosphere boundary (LAB) depth that could create our t* estimates. We found that the magnitude of our t* roughly corresponds to a LAB around 130 km. Direct constraints on LAB depth is difficult, although studies suggest an average LAB ~70 km in the western U.S. (Li et al., 2007). Cratonic lithosphere thicknesses are much larger and estimates range from 200-350 km (Artemieva and Mooney, 2002). Therefore, although our t* magnitudes are large, they are still within the range to be representative of the conditions within the continent.

5.2 Comparisons with previous studies

Past attenuation studies have resolved many features across the U.S. Since there are many techniques in use to determine different types of attenuation, it is not unusual to find substantial differences between resulting maps. However, many large-scale attenuation patterns are markedly similar regardless of technique. For example, our study, among others, displays dominantly low attenuation in the cratonic continent and generally high attenuation in the western U.S. (e.g., Mitchell, 1975; Warren and Shearer, 2002; Lawrence et al., 2006; Hwang et al., 2011; Pasyanos, 2013; Cafferky and Schmandt, 2015).

Smaller-scale lateral heterogeneities exist from study to study. For instance, our results indicate the North Basin and Range region displays relatively low attenuation. Cafferky and Schmandt (2015) found a similar pattern during their study, so it is unlikely that this feature is just an artifact from our technique. However, this feature is not present in early models (e.g., Mitchell 1975, Solomon and Toksöz, 1970), likely due to lack of

resolution prior to US-TA. Development of dense data arrays allow for more direct comparison between different techniques to resolve small-scale regional variations.

Additionally, our attenuation study can be related to velocity structure across the continent. Seismic velocity and attenuation have differing sensitivities to temperature, hydration, and partial melt (Dalton and Faul, 2010); therefore, comparing them produces stronger interpretations of upper mantle behavior associated with each parameter. Generally, large-scale patterns of velocity structures in the U.S. are characterized by fast anomalies in the thick, cold cratonic Midwest and slow speeds in the western U.S, Appalachian Mountains, and Ouachita Embayment (e.g., Obrebski et al., 2010; Schmandt and Lin, 2014; Shen and Ritzwoller, 2016; Porter et al., 2016). The transitions from high velocity to low velocity occur in approximately the same locations as transitions from low attenuation to high attenuation on our attenuation map. The correlation in transition location infers a strong relationship between attenuation and velocity structure.

Furthermore, seismic wave speed studies have strong lateral resolution, allowing for more specific regional comparisons with attenuation data. Schmandt and Lin (2014) offer a tomography study with multiple associations with observations from our attenuation map. For instance, the Ouachita Embayment region that displays relatively high attenuation in our study also corresponds to a regionally slow upper mantle velocity zone (Schmandt and Lin, 2014). Similar resemblances are present in Florida, New England, and Wyoming. Alternatively, the North Basin and Range region does not show the same correlation between attenuation and velocity. This area is characterized by low upper mantle velocities (e.g., Obrebski et al., 2011; Shen et al., 2013; Schmandt and Lin,

2014), yet we find relatively low t*. This disparity is indicative of regional dominance of non-thermally activated attenuation factors.

5.3 Significance of geographic attenuation variations

Attenuation appears to correspond with lithospheric strength. There are distinct t* gradients along the suture zones of the Trans-Hudson and Appalachian Front, however, cutting parallel to the Ouachita rifting zone gives more gradual disruptions in t*. This indicates the sharpness of the t* transition may be related to the tectonic processes that have dominated the region. The cratonic core is stronger than the accretionary provinces, which are shown to be more hydrous, fertile, and relatively weak (Whitmeyer and Karlstrom, 2007). The suture zones dominated by relatively narrow shear zones create similarly narrow transitions from low to high t*. Conversely, regions of extensional rifting perpendicular to the accretionary boundaries present broader, slower gradients in t*.

Seismic patterns across the U.S. also support this claim. Overall, seismicity is generally located in areas exhibiting relatively high attenuation (outside the craton), specifically, earthquakes concentrate on the edges of t* regions (Figure 11). The United States National Seismic Hazard map developed by USGS (Petersen et al., 2014) supports the seismic patterns we observe. Based on knowledge about tectonic activity, it is not particularly unexpected to find limited seismicity in the cratonic core. Observing seismicity outside of the craton supports the claim of weaker crust being west of the Rocky Mountain Front and east of the Appalachian Front. Therefore, we present further evidence that attenuation is correlated to lithospheric strength.

Heat flow measurements can also reveal insights into lithospheric behavior. Lithospheric heat flow is largely governed by thermal conduction, except in regions of active igneous intrusion or major tectonic motion (Oxburgh, et. al, 1978). Therefore, like oceanic lithosphere, age and heat flow relationships should reflect a decrease in heat flow with time resulting from conductive cooling. This explains why we see relatively low heat flow in the oldest parts of the U.S. continent and record higher temperatures in areas, such as the western U.S., that have experienced more recent episodes of magmatism and tectonics. However, these generalized relations become more complex in actual applications to specific North American provinces.

Comparing heat flow measurements to our apparent attenuation data reveals areas in which temperature is not the dominant factor on attenuation. As previously stated, temperature is a known factor controlling attenuation (e.g., Jackson et al., 1992, 2002; Karato, 2003), however, our results showed only a weak positive correlation. For instance, we measure relatively low t* in the North Basin and Range, which is not typical for a region exhibiting high heat flow. Furthermore, in the western U.S. there are considerable variations in t* laterally over an area where the heat flow is uniformly high. Low t* in this area implies attenuation is not thermally controlled in this region, and opens up the possibility of other controlling factors.

Magmatism patterns in the North Basin and Range may explain the unique apparent attenuation measured in this area, as well as a few other areas that are not well correlated with the heat flow patterns we observe. The magmatism results show interesting relationships with apparent attenuation patterns. Where there was past

magmatism, but none currently, attenuation is generally lower. Areas of recent magmatism are typically more attenuating. During the early volcanism period, there is frequent and pervasive volcanism in the North Basin and Range. However, the recent magmatic episode shows no trace, despite surrounding the area. Again, we observe the early magmatism occurring in a relatively low t* region. The last period of magmatism in this area may have dehydrated the lithospheric mantle (Hammond and Humphreys, 2000; Humphreys et al., 2003). Hydration plays an important role in attenuation, and may be the distinguishing factor that separates North Basin and Range from the rest of the western U.S.

In addition to the North Basin and Range, some regions are quite interesting because they do not coincide with what we would expect based on their tectonic history. It appears the lowest t* estimates are nestled between the southern arms of the Mid-continent Rift (MCR). This is intriguing because one would expect the oldest cratonic lithosphere of the Superior Province to exhibit lowest t* since its lithosphere is estimated to be among the thickest in the U.S. (Yuan and Romanowicz, 2010; Foster et al., 2014), the region demonstrates low heat flow (Blackwell et al., 1991), and tomography studies show high upper mantle shear velocities (Schmandt and Lin, 2014). We speculate the major magmatic events associated with the MCR system could explain why the Superior Province does not exhibit lowest t*. Voluminous basaltic eruptions likely depleted the mantle in a similar fashion as described in the North Basin and Range (Hammond and Humphreys, 2000; Dalton and Faul, 2010); however, in this instance, dehydrated mantle is associated with elevated attenuation as opposed to decreased attenuation in the North

Basin and Range, which suggests the possibility that dehydration can have different effects on regional attenuation depending on the preexisting thermal structure.

Due to its complex tectonic history, Wyoming displays a unique sequence of observations, as well. The Wyoming province experienced distinct modification by the processes associated with Farallon slab subduction (Liu et al., 2010). Subsequent subduction of the Shatsky conjugate beneath Wyoming at ~65 Ma generated basal erosion of the Wyoming craton and resulted in depleted mantle beneath the Wyoming craton (Humphreys et al., 2015). This slab-stacking architecture may be responsible for the unique attenuation, heat flow, and velocity patterns observed in Wyoming. Heat flow measurements (Figure 8) are generally hot in the western U.S., however, there is a NE-trending gap across Wyoming that exhibits relatively low heat flow. This same gap is visible in velocity structure (e.g., Schmandt and Lin, 2014) and, to some extent, our apparent attenuation map. Although this region has experienced significant alteration through Farallon tectonics, its signatures are more consistent with cratonic patterns despite the crustal loss event associated with the Shatsky conjugate.

The Central Valley of California stands out for a different reason as it is an expected low attenuation feature that appears to be missing from our map. There are clear signatures of this region in heat flow (Figure 8), velocity (Porter et al., 2016), and seismicity (Figure 11), but we do not see any clear patterns on the attenuation map. This is likely a result of lack of resolution due to smoothing of the model.

6 Conclusion

We have mapped apparent attenuation across the U.S. using teleseismic P-waves from 19 deep earthquakes. Our t* estimates largely follow anticipated trends, with some regional exceptions. Apparent attenuation appears to correspond to lithospheric strength, which is evident in the relationships between attenuation patterns and the orientations of lithospheric provinces.

The apparent attenuation patterns exhibit limited correlation with heat flow measurements, indicating the influence of non-thermal factors on t* estimates. The correlation between attenuation and heat flow varies regionally. Much of the western U.S. shows good correlation, however, the North Basin and Range shows relatively low correlation. Non-thermal attenuation factors, most likely dehydration of the upper mantle as a result of magmatism, overwhelm the influence of temperature in this region, resulting in relatively low attenuation.

Attenuation is complementary to other parameters used to describe the behavior of the continental lithosphere. In addition to heat flow, tomography, and lithospheric thickness studies, attenuation can be used to define the structures that result from tectonic processes in the lithosphere. Improved comprehension regarding structural heterogeneity in the continental lithosphere would assist in discerning elastic and anelastic contributions to attenuation. Furthermore, satisfactory understanding of attenuation must await data that constrain the deep structure of the upper mantle in order to generate robust constraints on where attenuation occurs in the mantle.

Illustrations

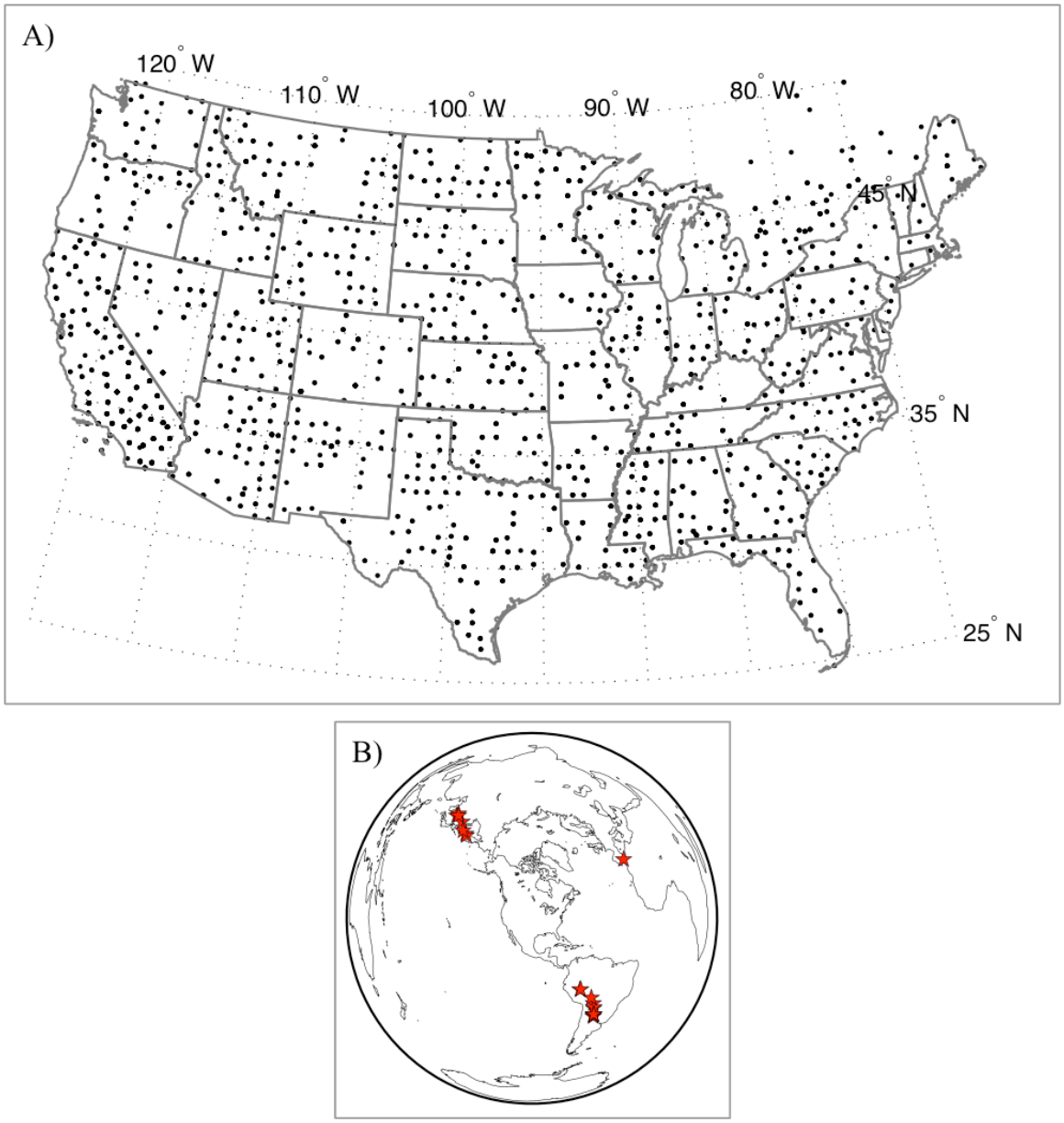

Figure 1. Station and event maps. A) The map shows station locations (circles) from US-TA used in the study. B) The global map shows the locations of the 19 deep earthquakes (red stars) used in this study.

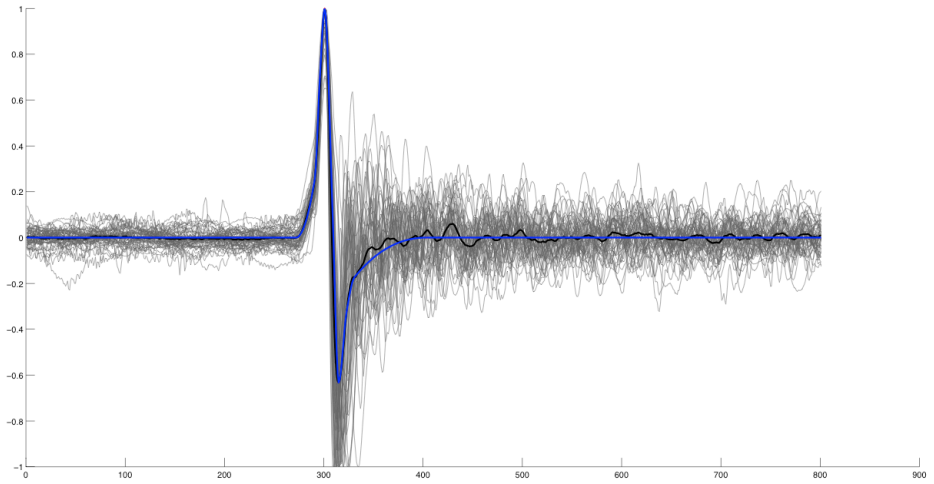

Figure 2. Sample source estimate for Mw 5.6 earthquake 502 km deep near southeast coast of Russia on 2012-07-29 recorded by 530 stations. Gray lines are 53 stacked traces that displayed clear, impulsive sources. Black line is the average of the stacked traces. Blue line is the traced source estimate for the event.

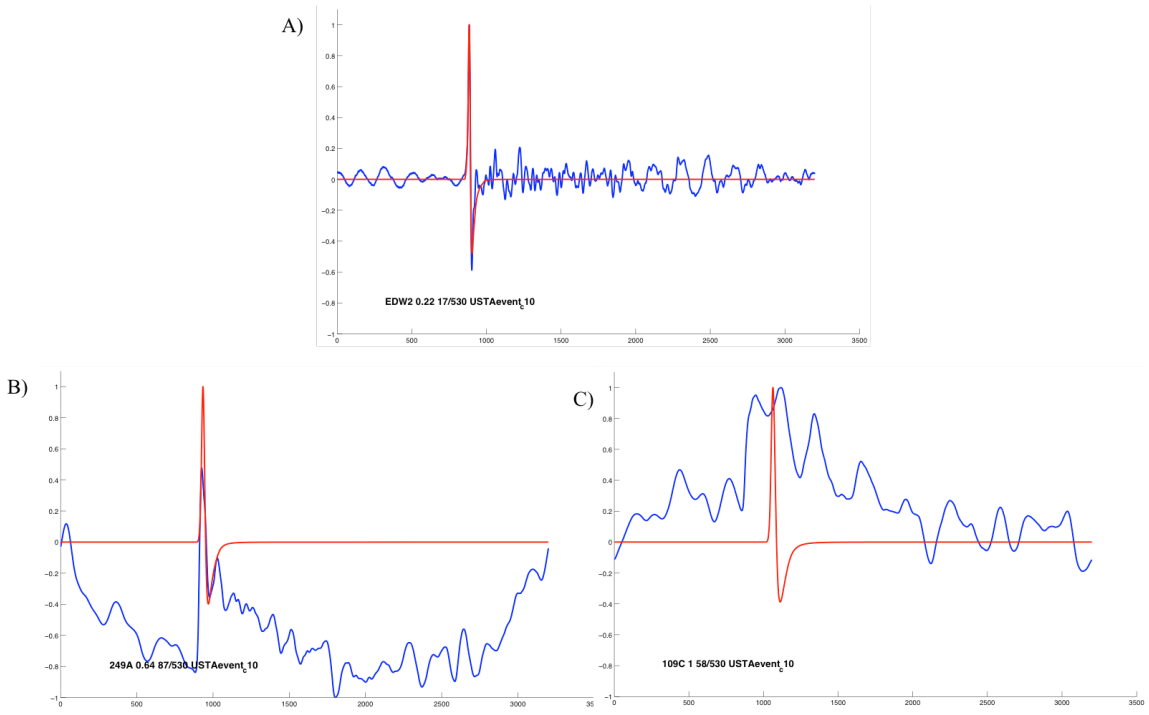

Figure 3. Examples comparing observed and attenuated source estimates for the same event described in Figure 2. Blue line represent the recorded signal at one station. Red line is the attenuated source estimate to fit the recorded trace. A) Demonstrates strong fit between station record and attenuated source estimate. We are not sensitive to the amount of energy in the coda, our focus is only on the source. B) Sample of a poor fit due to noisy record. The source estimate was fitted to a section of the record, but does not accurately represent the source. Therefore, records such as this were not included in the study. C) Particularly noisy records that showed no fit with the attenuated source estimate were removed from consideration, as well.

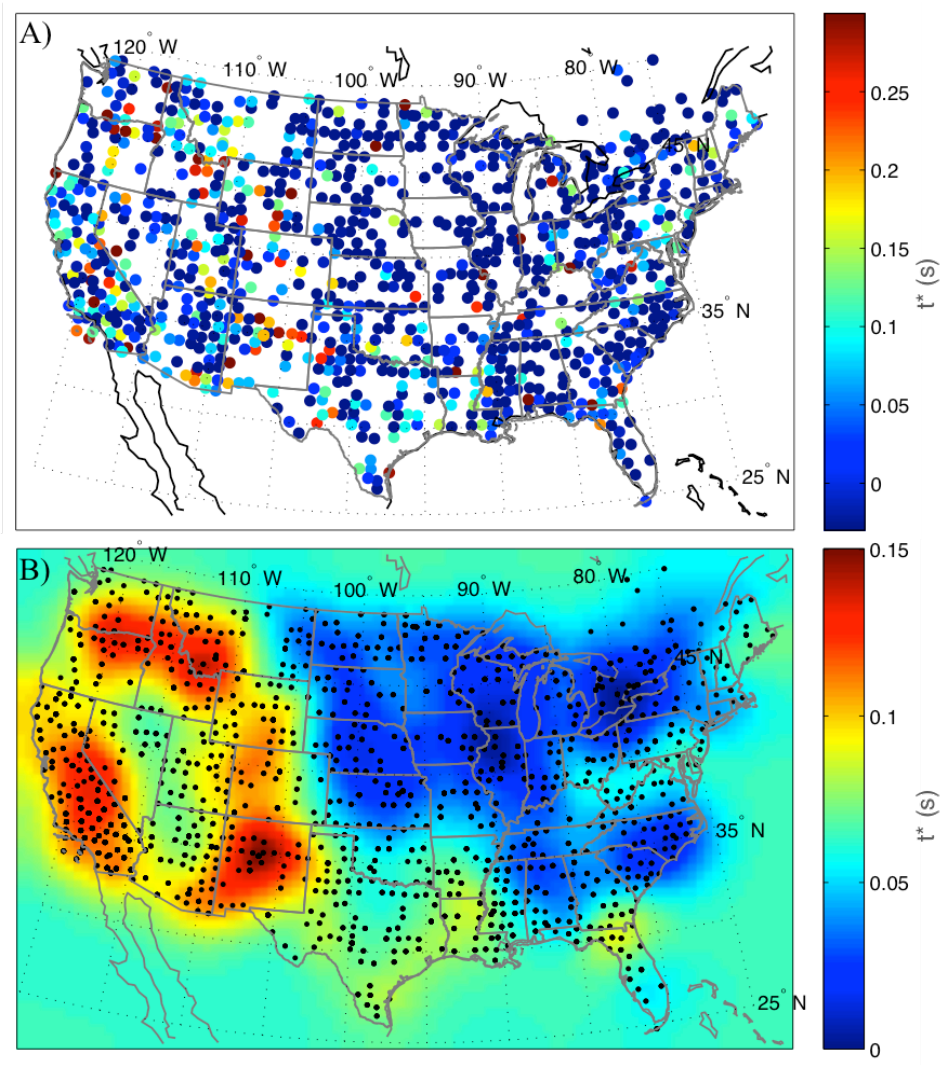

Figure 4. Raw and smoothed t* maps. A) t* for each station. Station terms absorb the local attenuation structure and are a vital piece of the inversion. B) The map shows a smoothed surface of t*. Black circles are station locations. Note the colorbars for A) and B) have different scales for t*.

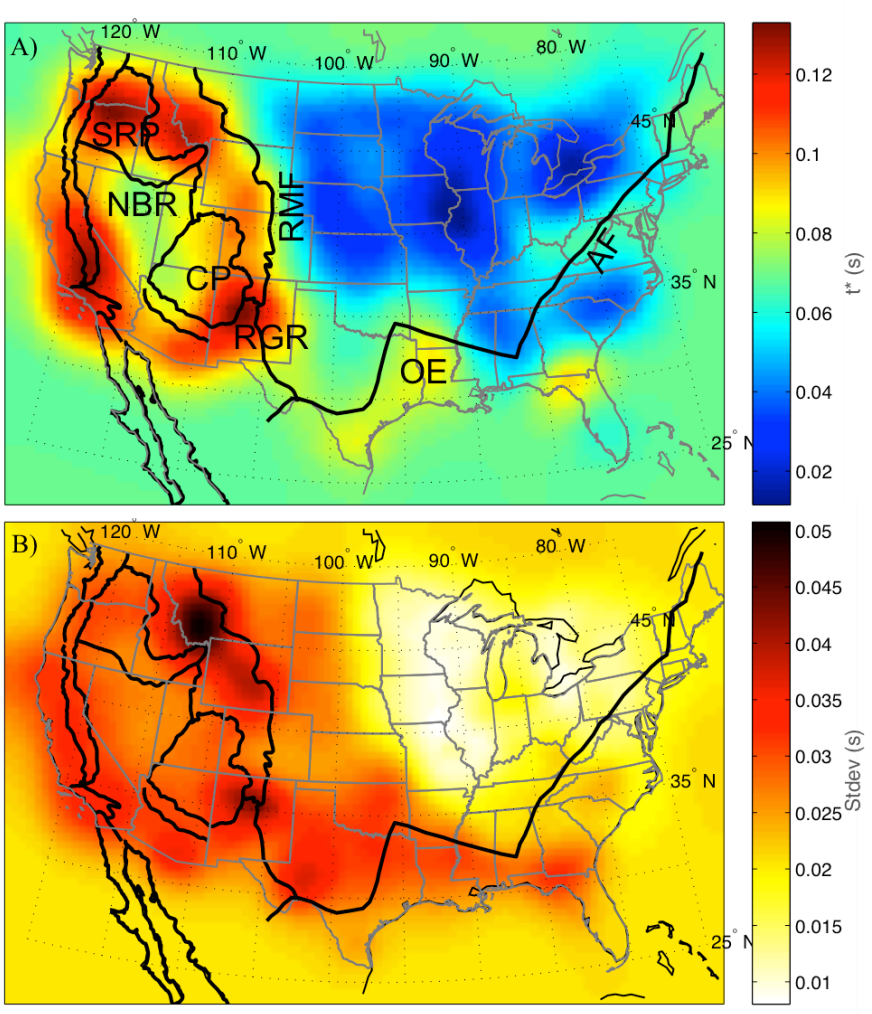

Figure 5. Jackknife test and standard deviation for 10/19 events. A) Stack and average 100 random combinations of 10/19 events. The locations of tectonic boundaries and provinces are labeled with black lines. The Appalachian front (AF) and Ouachita Embayment (OE) are inferred from Whitmeyer and Karlstrom (2007). Rocky Mountain front (RMF), Rio Grande Rift (RGR), Colorado Plateau (CP), Wyoming province (WP), North Basin and Range (NBR), and Snake River Plain (SRP) are labeled. B) Standard deviation map of the jackknife results with the same provinces as (A) for spatial reference.

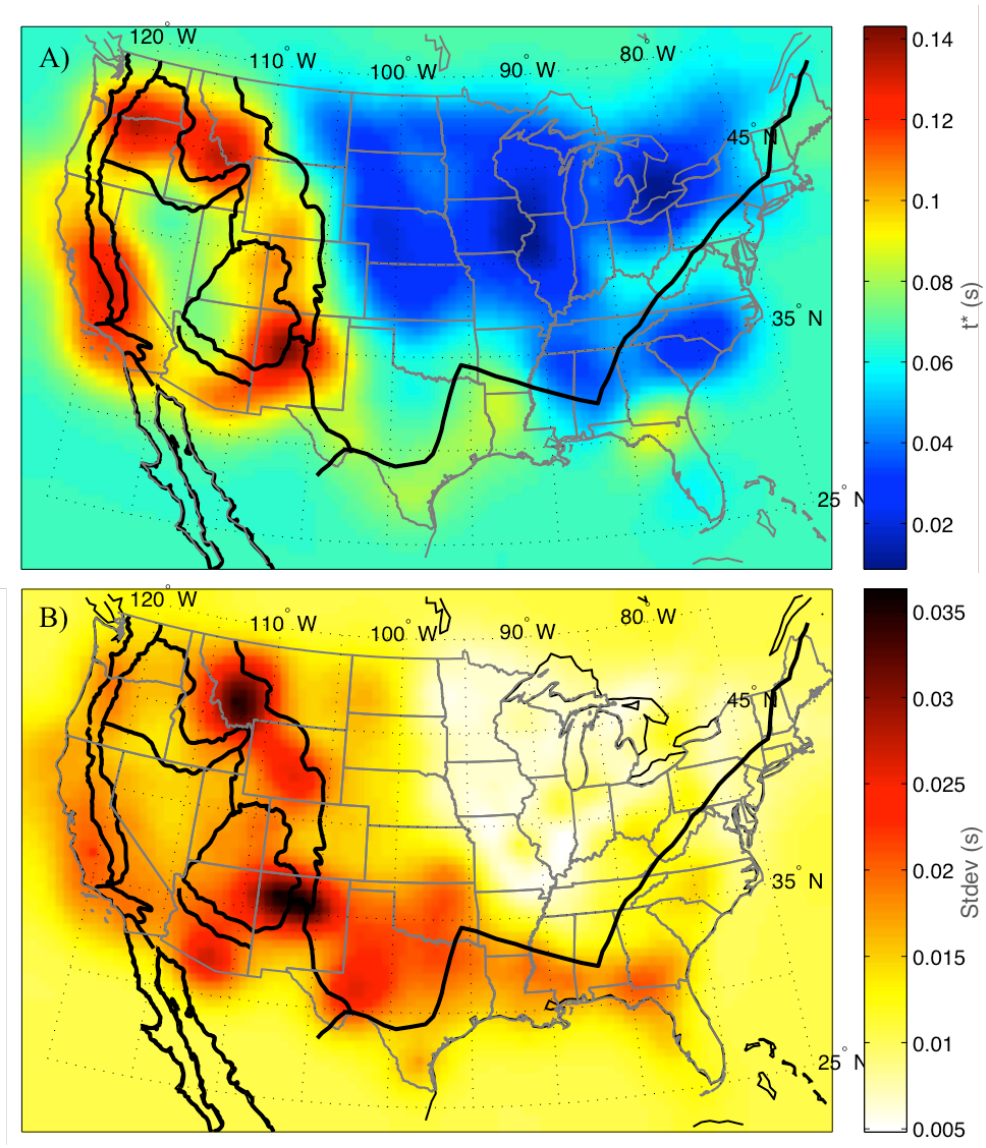

Figure 6. Jackknife with 14/19 event combinations. A) Same as figure 5 (A) except with 14 random events of the possible 19. B) Standard deviation map for the jackknife of 14/19 events. The same provinces from figure 5 are present to serve as reference.

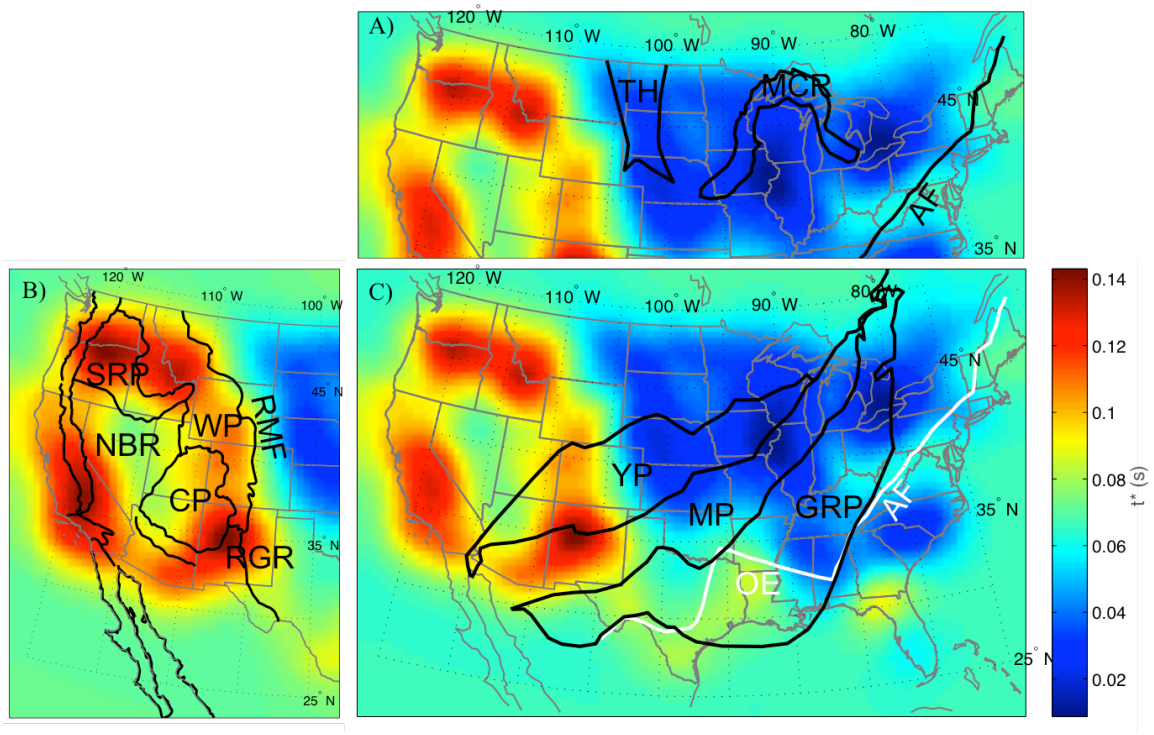

Figure 7. Noteworthy boundaries and provinces with attenuation base map. A) Provinces labeled on the t* map resulting from the jackknife (10/19 events). Shows Trans-Hudson (TH) inferred from Foster et al. (2014); Mid-Continent Rift (MCR), inferred from Stein et al. (2011); and Appalachian front (AF). B) Shows western US provinces, previously labeled in figure 5. C) NE-trending provinces are labeled. Yavapai province (YP), Mazatzal province (MP), and Granite-Rhyolite province (GRP), inferred from Whitmeyer and Karlstrom (2007) are outlined in black. The white line represents the Appalachian front (AF). The location of the Ouachita Embayment (OE) is labeled, as well.

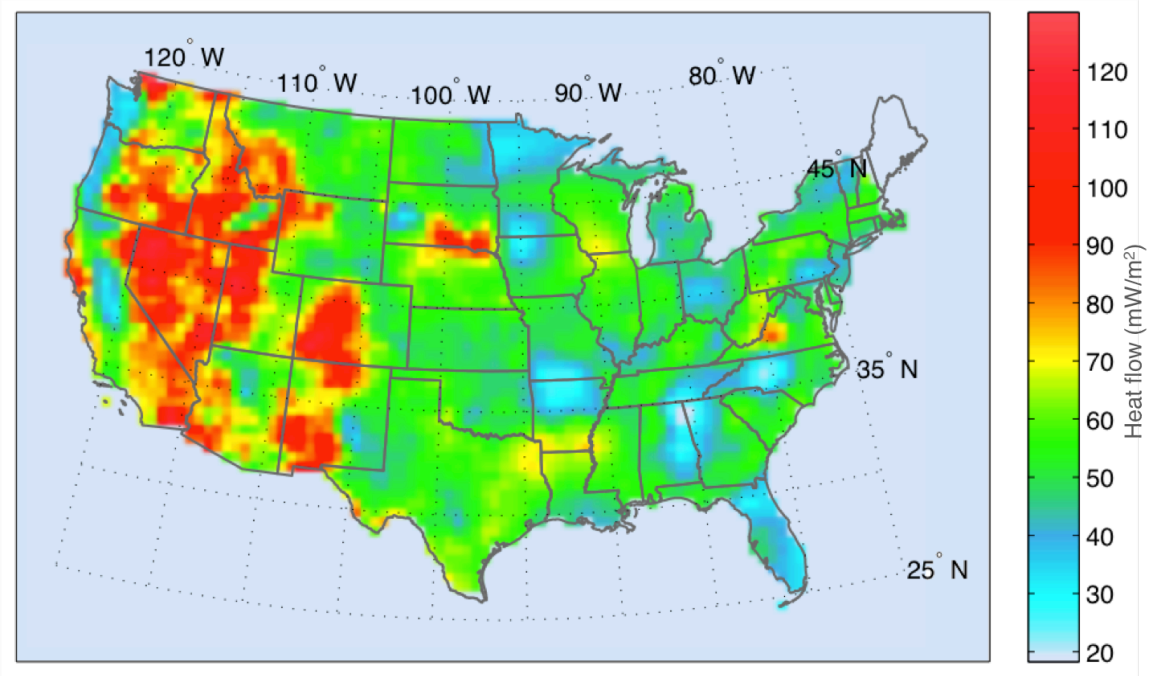

Figure 8. Geothermal map of North America reprocessed from Blackwell et al. (2011).

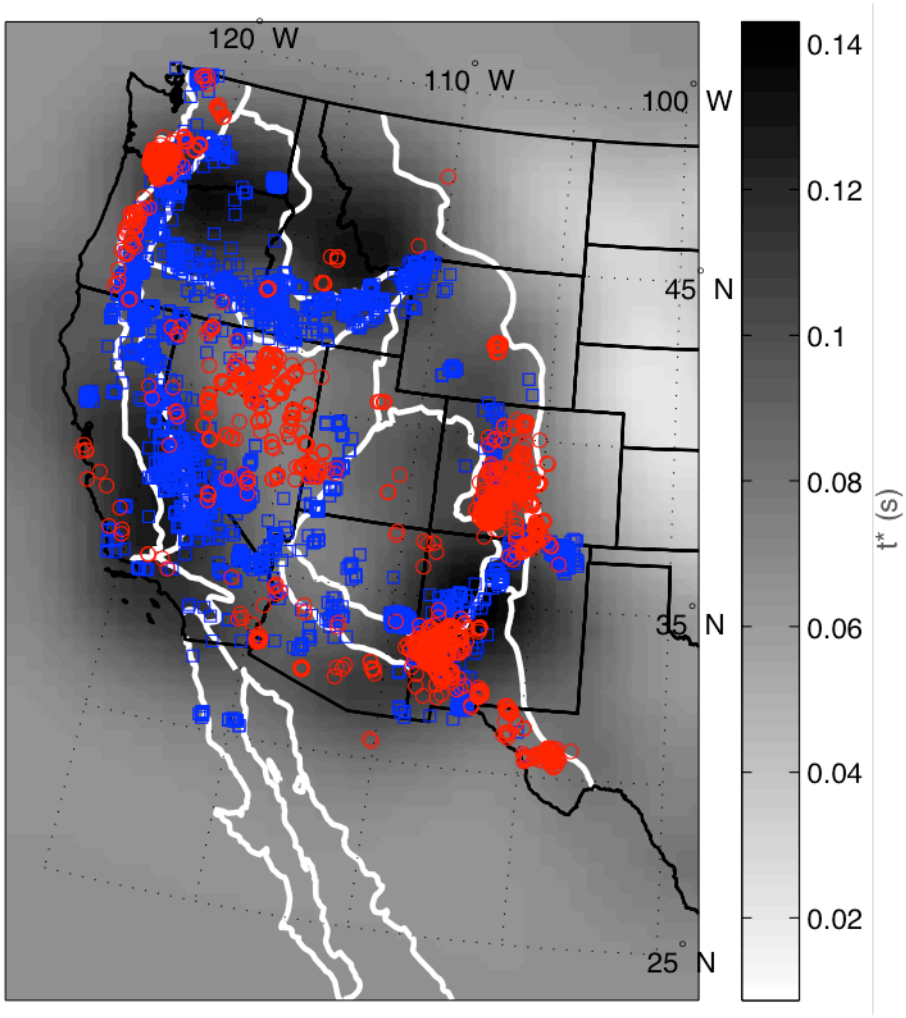

Figure 9. NAVDat magmatic data in the western U.S. with t* base map. Red circles represent magmatism from 45-21 Ma. Blue squares represent magmatism from 20-0 Ma. The western provinces are in white for reference.

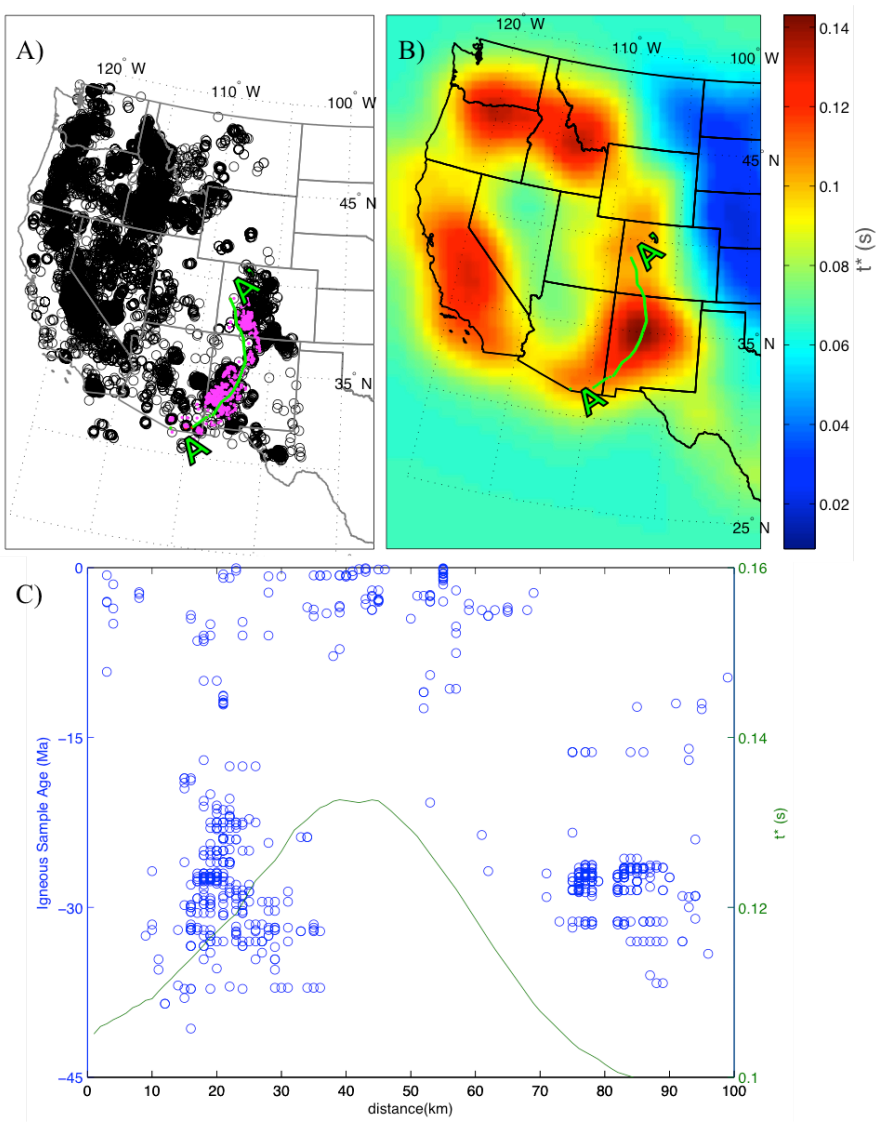

Figure 10. Rio Grande Rift magmatism. A) NAVDat data plotted in black circles. A-A' (green line) marks the location of the Rio Grande Rift (RGR). Magenta dots are the igneous samples associated with the Rio Grande Rift. B) t* map of the western U.S. A-A' transect plotted in green. C) Plot of RGR-associated igneous sample ages (blue circles) compared to t* estimates (green line) along the A-A' transect. Early magmatism (45-21 Ma) occurs mostly outside the peak attenuation region, creating a gap roughly correlated with highest t*. Recent magmatism (20-0 Ma) fills in that gap.

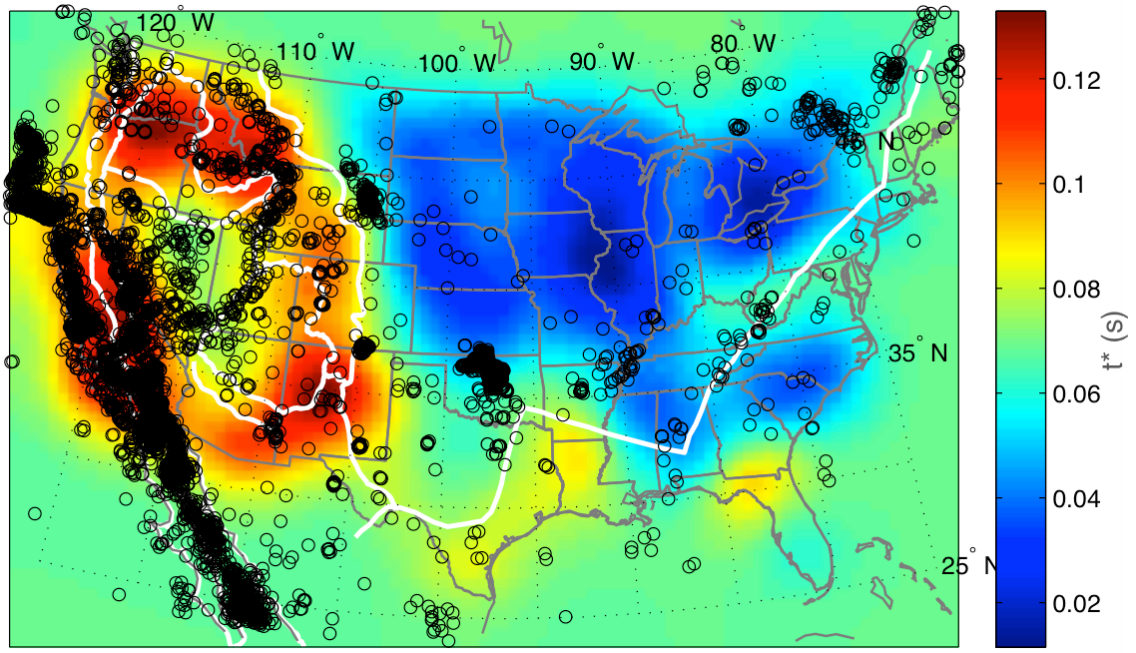

Figure 11. U.S. seismicity distribution with t* base map. Black circles represent 10 years of seismic data (1996-2016), with Appalachian front and western provinces for reference. Earthquake locations appear to concentrate around the borders of Q regions.

Bibliography

Artemieva, I. M., & Mooney, W. D. (2002). On the relations between cratonic lithosphere thickness, plate motions, and basal drag. *Tectonophysics*, *358*(1), 211-231.

Atwater, T. (1970). Implications of plate tectonics for the Cenozoic tectonic evolution of western North America. *Geological Society of America Bulletin*, *81*(12), 3513-3536.

Azimi S.A., Kalinin A.V., Kalinin V.V. and Pivovarov B.L., 1968. Impulse and transient characteristics of media with linear and quadratic absorption laws. *Izv. Earth Physics*, 42-54.

Blackwell, D. D., 1971, The thermal structure of the continental crust, *in* Heacock, J. G., ed., The structure and physical properties of the Earth's crust: American Geophysical Union Monograph 14, p. 169-184.

Blackwell, D. D., Steele, J. L., & Carter, L. S. (1991). Heat flow patterns of the North American continent: A discussion of the DNAG geothermal map of North America. *Neotectonics of North America*, *1*, 423-437.

Blackwell, D. D., Richards, M. C., Frone, Z. S., Batir, J. F., Williams, M. A., Ruzo, A. A., and Dingwall, R. K., 2011, "SMU Geothermal Laboratory Heat Flow Map of the Conterminous United States, 2011". Supported by Google.org. Available at http://www.smu.edu/geothermal.

Cafferky, S., & Schmandt, B. (2015). Teleseismic P wave spectra from USArray and implications for upper mantle attenuation and scattering.*Geochemistry, Geophysics, Geosystems*, *16*(10), 3343-3361.

Corrigan, D., Hajnal, Z., Nemeth, B., and Lucas, S.B., 2005, Tectonic framework of a Paleoproterozoic arc-continent to continent-continent collisional zone, Trans-Hudson Orogen, from geological and seismic reflection studies: Canadian Journal of Earth Sciences, v. 42, p. 421–434, doi: 10.1139/ e05-025.

Dalton, C. A., Ekström, G., & Dziewoński, A. M. (2008). The global attenuation structure of the upper mantle. *Journal of Geophysical Research: Solid Earth*, *113*(B9).

Dalton, C. A., and U. H. Faul (2010), The oceanic and cratonic upper mantle: Clues from joint interpretation of global velocity and attenuation models, Lithos, 120, 160–172.

Dickinson, W. R. (2002), The Basin and Range province as a composite extensional domain, *Int. Geol. Rev., 44,* 1-38, doi:10.2747/00206814.44.1.1.

Dziewonski, A. M., & Anderson, D. L. (1981). Preliminary reference Earth model. *Physics of the earth and planetary interiors*, *25*(4), 297-356.

Faul, U. H., & Jackson, I. (2005). The seismological signature of temperature and grain size variations in the upper mantle. *Earth and Planetary Science Letters*, *234*(1), 119-134.

Foster, K., Dueker, K., Schmandt, B., & Yuan, H. (2014). A sharp cratonic lithosphere–asthenosphere boundary beneath the American Midwest and its relation to mantle flow. *Earth and Planetary Science Letters*, *402*, 82-89.

Goes, S., and S. van der Lee (2002), Thermal structure of the North American uppermost mantle inferred from seismic tomography, *J. Geophys. Res.*, 107(B3), 2050, doi:10.1029/2000JB000049.

Gung, Y., & Romanowicz, B. (2004). Q tomography of the upper mantle using three-component long-period waveforms. *Geophysical Journal International*,*157*(2), 813-830.

Hammond, W. C., and E. D. Humphreys (2000), Upper mantle seismic wave attenuation: Effects of realistic partial melt distribution, *J. Geophys. Res.*, 105, 10,987–10,999.

Hoffman, P.F., 1988, United plates of America, the birth of a craton; early Proterozoic assembly and growth of Laurentia: Annual Review of Earth and Planetary Sciences, v.16, p.543–603, doi: 10.1146/annurev. ea.16.050188.002551.

Humphreys, E. D., and Dueker, K. G., 1994, Physical state of the western U.S. mantle: Journal of Geophysical Research, v. 99, p. 9635-9650.

Humphreys, E., E. Hessler, K. Dueker, G. L. Farmer, E. Erslev, and T. Atwater (2003), How Laramide-age hydration of North American lithosphere by the Farallon slab controlled subsequent activity in the western United States, *Int. Geol. Rev.*, 45, 575–595.

Humphreys, E. D., Schmandt, B., Bezada, M. J., & Perry-Houts, J. (2015). Recent craton growth by slab stacking beneath Wyoming. *Earth and Planetary Science Letters*, *429*, 170-180.

Hwang, Y. K., J. Ritsema, and S. Goes (2011), Global variation of body-wave attenuation in the upper mantle from teleseismic P wave and S wave spectra, Geophys. Res. Lett.,38, L06308, doi:10.1029/2011GL046812.

Jackson, I., M. S. Paterson, and J. D. Fitz Gerald (1992), Seismic wave attenuation in Aheim dunite: An experimental study,*Geophys. J. Int.*, 108, 517–534.

Jackson, I., J. D. Fitz Gerald, U. H. Faul, and B. H. Tan (2002), Grain-size-sensitive seismic wave attenuation in polycrystalline olivine, *J. Geophys. Res.*, 107(B12), 2360, doi:10.1029/2001JB001225.

Karato, S. I. (2003). Mapping water content in the upper mantle. *Inside the subduction factory*, 135-152.

Karlstrom, K.E., and Bowring, S.A., 1988, Early Proterozoic assembly of tectonostratigraphic terranes in southwestern North America: Journal of Geology, v. 96, p. 561–576.

Karlstrom, K. E., & Humphreys, E. D. (1998). Persistent influence of Proterozoic accretionary boundaries in the tectonic evolution of southwestern North America. *Rocky Mountain Geology*, *33*(2), 161-179.

Lawrence, J. F., P. M. Shearer, and G. Masters (2006), Mapping attenuation beneath North America using waveform cross-correlation and cluster analysis, Geophys. Res. Lett., 33, L07315, doi:10.1029/2006GL025813.

Li, X., Yuan, X., & Kind, R. (2007). The lithosphere-asthenosphere boundary beneath the western United States. *Geophysical Journal International*,*170*(2), 700-710.

Liu, L., Gurnis, M., Seton, M., Saleeby, J., Müller, R. D., & Jackson, J. M. (2010). The role of oceanic plateau subduction in the Laramide orogeny. *Nature Geoscience*, *3*(5), 353-357.

McQuarrie, N., and M. Oskin (2010), Palinspastic restoration of NAVDat and implications for the origin of magmatism in southwestern North America, J. Geophys. Res., 115, B10401, doi:10.1029/2009JB006435.

Mitchell, B. J. (1975). Regional Rayleigh wave attenuation in north America. *Journal of Geophysical Research*, *80*(35), 4904-4916.

Mitchell, B. J. (1995). Anelastic structure and evolution of the continental crust and upper mantle from seismic surface wave attenuation. *Reviews of Geophysics*, *33*(4), 441-462.

Moores, E. M. (1991). Southwest US-East Antarctic (SWEAT) connection: a hypothesis. *Geology*, *19*(5), 425-428.

Morgan, P., & Gosnold, W. D. (1989). Heat flow and thermal regimes in the continental United States. *Geological Society of America Memoirs*, *172*, 493-522.

Obrebski, M., Allen, R. M., Pollitz, F., & Hung, S. H. (2011). Lithosphere–asthenosphere interaction beneath the western United States from the joint inversion of body-wave traveltimes and surface-wave phase velocities. *Geophysical Journal International*, *185*(2), 1003-1021.

Oxburgh, E. R., Parmentier, E. M., Froidevaux, C., & Harte, B. (1978). Thermal processes in the formation of continental lithosphere [and discussion]. *Philosophical Transactions of the Royal Society of London A: Mathematical, Physical and Engineering Sciences*, *288*(1355), 415-429.

Pasyanos, M. E. (2013). A lithospheric attenuation model of North America. *Bulletin of the Seismological Society of America*.

Petersen, M.D., Moschetti, M.P., Powers, P.M., Mueller, C.S., Haller, K.M., Frankel, A.D., Zeng, Yuehua, Rezaeian, Sanaz, Harmsen, S.C., Boyd, O.S., Field, Ned, Chen, Rui, Rukstales, K.S., Luco, Nico, Wheeler, R.L., Williams, R.A., and Olsen, A.H., 2014, Documentation for the 2014 update of the United States national seismic hazard maps: U.S. Geological Survey Open-File Report 2014–1091, 243 p., *http://dx.doi.org/10.3133/ofr20141091*.

Porter, R., Y. Liu, and W. E. Holt (2016), Lithospheric records of orogeny within the continental U.S., Geophys. Res. Lett., 43, 144–153, doi:10.1002/2015GL066950.

Romanowicz, B. (1995). A global tomographic model of shear attenuation in the upper mantle. *Journal of Geophysical Research: Solid Earth*, *100*(B7), 12375-12394.

Roth, E. G., Wiens, D. A., Dorman, L. M., Hildebrand, J., & Webb, S. C. (1999). Seismic attenuation tomography of the Tonga-Fiji region using phase pair methods. *Journal of Geophysical Research: Solid Earth*, *104*(B3), 4795-4809.

Roy, R. F., Blackwell, D. D., and Decker, E.R., 1972, Continental heat flow, *in* Robertson, E. C., ed., The nature of the solid earth: New York, McGraw-Hill, p.506-543.

Sass, J. H., A. H. Lachenbruch, R. J. Munroe, G. W. Greene, and T. H. Moses Jr. (1971), Heat flow in the western United States, J. Geophys. Res., 76(26), 6376–6413, doi:10.1029/JB076i026p06376.

Schmandt, B., & Lin, F. C. (2014). P and S wave tomography of the mantle beneath the United States. *Geophysical Research Letters*, *41*(18), 6342-6349.

Selby, N. D., & Woodhouse, J. H. (2002). The Q structure of the upper mantle: Constraints from Rayleigh wave amplitudes. *Journal of Geophysical Research: Solid Earth*, *107*(B5).

Shen, W., M. H. Ritzwoller, and V. Schulte-Pelkum (2013), A 3-D model of the crust and uppermost mantle beneath the central and western US by joint inversion of receiver functions and surface wave dispersion, J. Geophys. Res., 118(1), 262–272, doi:10.1029/2012JB009602.

Shen, W., & Ritzwoller, M. H. (2016). Crustal and uppermost mantle structure beneath the United States. *Journal of Geophysical Research: Solid Earth*.

Solomon, S. C., and Toksöz, M. N. (1970), Lateral variation of attenuation of P and S waves beneath the United States. *Bulletin of the Seismological Society of America*, 60: 819-838.

Stein, et. al (2011), Learning from failure: The SPREE Mid-Continent Rift Experiment, GSA Today, 21(9), doi: 10.1130/G120A.1.

Walker, J. D., T. D. Bowers, A. F. Glazner, G. L. Farmer, and R. W. Carlson (2004), Creation of a North American volcanic and plutonic rock data- base (NAVDAT), Geol. Soc. Am. Abstr. Programs, 36(4), 9.

Warren, L. M., & Shearer, P. M. (2002). Mapping lateral variations in upper mantle attenuation by stacking P and PP spectra. *Journal of Geophysical Research: Solid Earth*, *107*(B12).

Whitmeyer, S. J., & Karlstrom, K. E. (2007). Tectonic model for the Proterozoic growth of North America. *Geosphere*, *3*(4), 220-259.

Wiens, D. A., Conder, J. A., & Faul, U. H. (2008). The seismic structure and dynamics of the mantle wedge. *Annu. Rev. Earth Planet. Sci.*, *36*, 421-455.

Yuan, H., & Romanowicz, B. (2010). Lithospheric layering in the North American craton. *Nature*, *466*(7310), 1063-1068.